MITSUBISHI ELECTRIC RESEARCH LABORATORIES
http://www.merl.com

Multiscale Energy Products for TOA Estimation in IR-UWB Systems

I. Guvenc, Z. Sahinoglu

TR2005-042 December 2005

Abstract

In this paper, we consider time of arrival estimation of ultra-wideband signals based on low-rate samples that are obtained after a square-law device. Signal conditioning techniques based on a bank of cascaded multi-scale energy collection filters and wavelets are introduced, where correlations across multiple scales are exploited for edge and peak enhancements towards a more accurate detection. The performances of the discussed algorithms are tested on IEEE802.15.4a residential line-of-sight (LOS) channels.

IEEE Globecom, November 2005

Multiscale Energy Products for TOA Estimation in IR-UWB Systems

I. Guvenc[1,2] and Z. Sahinoglu[1]
[1]Mitsubishi Electric Research Labs, 201 Broadway Ave., Cambridge, MA, 02139
[2]Department of Electrical Engineering, University of South Florida, Tampa, FL, 33620
E-mail:{guvenc, zafer}@merl.com

***Abstract*— In this paper, we consider time of arrival estimation of ultra-wideband signals based on low-rate samples that are obtained after a square-law device. Signal conditioning techniques based on a bank of cascaded multi-scale energy collection filters and wavelets are introduced, where correlations across multiple scales are exploited for edge and peak enhancements towards a more accurate detection. The performances of the discussed algorithms are tested on IEEE 802.15.4a residential line-of-sight (LOS) channels.**

I. Introduction

High time resolution is one of the key benefits of impulse radio ultra-wideband (IR-UWB) signals for precision ranging. Due to extremely short duration of transmitted UWB pulses, UWB receivers, as opposed to typical narrow-band wireless receivers, enjoy being able to resolve individual multipath components; and the accuracy of TOA estimation is characterized by how finely the first arriving signal path is identified, which may not be the strongest.

Matched filtering (MF), where a correlator template exactly matches to the received signal, is the optimum filtering technique for signal detection. However, UWB receivers typically have to operate at sub-Nyquist sampling rates; this makes it difficult to align with the various multipath components of the received signal for MF implementation. Another practical concern for MF is the requirement to have *a-priori* knowledge of the received pulse shapes, which may change from an environment to another and even between different multipath components [1]. Therefore, it is difficult to exactly match to the received pulse-shape, especially when considering the analog implementations of the template waveforms.

Typical approaches for UWB ranging in the literature are based on MF of the received signal. Corresponding the time index that maximizes the MF output to the TOA estimate is probably the simplest timing estimation technique [2]-[5]. These approaches have limited TOA precision, as the strongest path is not necessarily the first arriving path. In order to determine the leading edge of a received signal, Lee and Scholtz proposed to use a generalized maximum-likelihood (GML) approach to search the paths prior to the strongest path [6]. In [7], the leading edge detection problem is taken as a break-point estimation of the actual signal itself, where temporal correlation arising from the transmitted pulse is used to accurately partition the received signal. In both [6], [7], very high sampling rates were considered, which may not be practical in many scenarios. A two-step ranging algorithm is considered in [8] to decrease sampling rate requirements, where an energy detection (ED) step gives coarse information about the signal's whereabouts, and a MF step is applied into the detected energy block(s) for refinement.

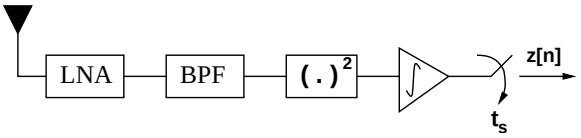

Fig. 1. Sampling of the received signal after energy detection.

Due to above practical concerns and limitations with MF at low rate samples, ED based ranging becomes a feasible alternative. Even though it suffers more from noise due to a square-law device, ED does not require accurate timing or pulse shapes. In [9], a synchronization analysis using EDs shows the potential of non-coherent reception for timing estimation in IR-UWB systems.

In this paper, we consider TOA estimation based on ED of the received signal at sub-Nyquist rate sampling. Signal conditioning methods are introduced, where a bank of cascaded energy collection filters are used to exploit the temporal cross-scale correlation and enhance the accuracy of maximum energy selection (MES). Multiscale energy product of the appropriately designed filter outputs is shown to enhance and shift the peak sample closer to the leading edge. The performance of a modified Mallat-Zhong discrete wavelet transform (MZ-DWT) [10], [11] is investigated for edge detection, whose accuracy is not as satisfactory due to non-sharp edges and multiple clusters of the multipath components. Also, a filtering technique is discussed which enhances the peak selection by exploiting the energy and information within neighboring samples. Simulation results demonstrate the improvements in the mean absolute error (MAE) of TOA estimation when the proposed algorithms are employed.

II. System Model

Let the received UWB multipath signal be represented as

$$r(t) = \sum_{j=-\infty}^{\infty} d_j \omega_{mp}\big(t - jT_f - c_j T_c - \tau_{toa}\big) + n(t) \quad (1)$$

where frame index and frame duration are denoted by j and T_f, N_s represents the number of pulses per symbol, T_c is the chip duration, T_s is the symbol duration, τ_{toa} is the TOA of the received signal, and N_h is the possible number of chip positions per frame, given by $N_h = T_f/T_c$. Effective pulse after the channel impulse response is given by $\omega_{mp}(t) =$

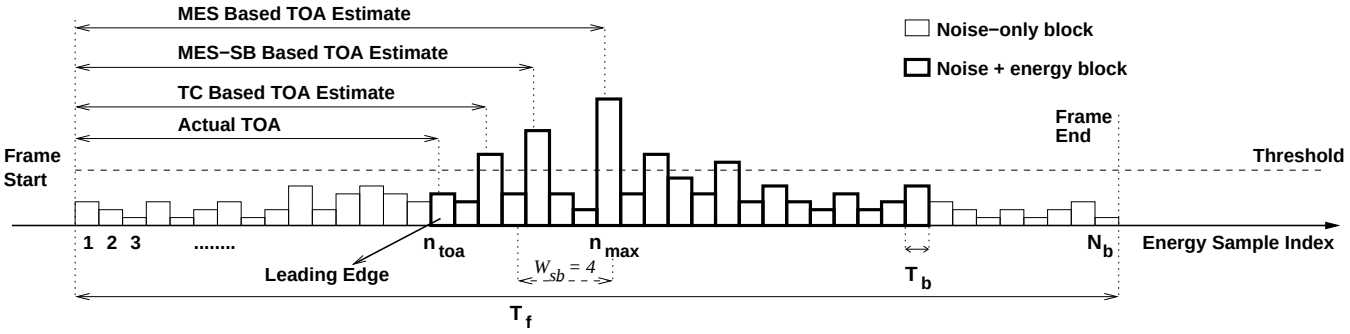

Fig. 2. Illustration of basic TOA estimation techniques based on energy samples.

$\sqrt{E}\sum_{l=1}^{L}\alpha_l\omega(t-\tau_l)$, where $\omega(t)$ is the received UWB pulse with unit energy, E is the pulse energy, α_l and τ_l are the fading coefficients and delays of the multipath components, respectively. Additive white Gaussian noise (AWGN) with zero-mean and double-sided power spectral density $\mathcal{N}_0/2$ and variance σ^2 is denoted by $n(t)$. The time-hopping codes and random polarity codes are denoted by $c_j \in \{0,\ 1, ..., N_h - 1\}$ and $d_j \in \{\pm 1\}$, respectively. No modulation is considered for the ranging process.

A. Sampling of the Received Signal After a Square-law Device

In the sequel, we assume that a coarse acquisition on the order of frame-length is acquired in (1), such that $\tau_{toa} \sim \mathcal{U}(0, T_f)$, where $\mathcal{U}(.)$ denotes the uniform distribution. As for the search region, the signal within time frame T_f plus half of the next frame is considered to factor-in inter-frame leakage due to multipath, and the signal is then input to a square-law device with an integration interval of $t_s = T_b$ (see Fig. 1). The number of samples (or blocks) is denoted by $N_b = \frac{3}{2}\frac{T_f}{T_b}$, and $n \in \{1,\ 2, ..., N_b\}$ denotes the sample index with respect to the starting point of the uncertainty region (inter-pulse interference is neglected). The samples at the output of the square-law device are given by[1]

$$z[n] = \sum_{j=1}^{N_s} \int_{(j-1)T_f+(c_j+n-1)T_b}^{(j-1)T_f+(c_j+n)T_b} |r(t)|^2 dt \ , \qquad (2)$$

and the performance can be further improved by using the energy in N_T symbols. The bit energy when using N_s pulses becomes $E_b = N_s E$.

B. Design Trade-offs

There exists a trade-off between using larger blocks and smaller blocks in energy detection. As the block size gets narrower individual peaks due to noise increases the likelihood of leading-energy block misdetection. Besides, there is a trade-off between using multiple pulses per symbol and a single (or few) pulse(s) with an equivalent energy. In Table I, statistics of the energy detector outputs for noise-only samples (i.e., μ_0 and σ_0^2), and signal plus noise samples (i.e., μ_n and σ_n^2 for the nth sample)) are given for single and multiple pulses per symbol to demonstrate the impact of N_s on the performance. Degree of freedom is given by $M = 2BT_b + 1$, E_n is the total signal energy within the nth block, and B is the signal bandwidth. Careful observation of the table reveals that the *mean-shifts* between μ_0 and μ_n for the two cases are identical, i.e. $N_s E_n$. However, when multiple pulses are employed, the noise variances corresponding to both noise-only and signal plus noise blocks increases. This implies that leading edge detection algorithm will perform detrimental as the number of pulses increases.

TABLE I
STATISTICS FOR SINGLE AND MULTIPLE PULSES PER SYMBOL.

	Single pulse	**Multiple pulses**
μ_0	$M\sigma^2$	$N_s M\sigma^2$
σ_0^2	$2M\sigma^4$	$2N_s M\sigma^4$
μ_n	$M\sigma^2 + N_s E_n$	$N_s M\sigma^2 + N_s E_n$
σ_n^2	$2M\sigma^4 + 4\sigma^2 N_s E_n$	$2N_s M\sigma^4 + 4\sigma^2 N_s E_n$

Also note that the selection of $N_b * T_b = T_f$ limits the maximum measurable distance. For instance, a distance that it would take $(N_b + 1) * T_b$ seconds for the radio frequency (RF) signal to traverse would be erroneously treated as a signal arriving within the first block in the energy analysis.

In the next two sections, basic TOA estimation algorithms (see Fig. 2) as well as proposed techniques that operate on $z[n]$ for leading edge detection are presented and formulated.

III. TOA Estimation Algorithms

Choosing the maximum energy output to be the leading edge is the simplistic way of achieving a timing estimate. Using MES, the TOA estimate with respect to the beginning of the time frame is evaluated as $\hat{t}_{MES} = \Big[\underset{1\le n\le N_b}{\operatorname{argmax}}\big\{z[n]\big\}\Big]T_b = n_{max}T_b$. However, the strongest energy block in many cases may not be the leading energy block (Fig. 2), and the MES therefore hits an error-floor even in high signal to noise ratio (SNR) region. Also, the performance of it degrades with uncertainiry region N_b, since it becomes more likely to identify a noise only block as the maximum energy block.

Received samples can be also compared to an appropriate threshold, and the first threshold-exceeding sample index can be corresponded as the TOA estimate, i.e. $\hat{t}_{TC} = \Big[\min\big\{n|z[n] > \xi\big\}\Big]T_b$, where ξ is a threshold that must be set based on the received signal statistics. Given the minimum

[1]Note that chip-rate (or other high-rate) sampling can be achieved by using symbol-spaced sampling and multiple training symbols, and shifting the signal by desired sampling period at each symbol.

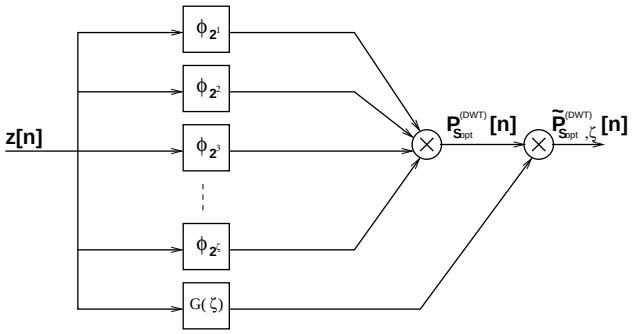

Fig. 3. Block diagram for weighted multi-scale product of MZ-DWT.

and maximum energy sample values, the following normalized threshold can be used [12]

$$\xi_{norm} = \frac{\xi - \min\{z[n]\}}{\max\{z[n]\} - \min\{z[n]\}} \ . \tag{3}$$

In order to improve the performance of the MES, the samples prior to the maximum energy sample can be searched. The TOA estimate with such a searchback and thresholding scheme is then given by $\hat{t}_{MES-SB} = \Big[\min\{n|\tilde{z}[n] > \xi\} + n_{max} - W_{sb} - 1\Big] T_b$, where $\tilde{z}[n] = \Big[z[n_{max} - W_{sb}] \ z[n_{max} - W_{sb} + 1] \ \ \ldots \ \ z[n_{max}]\Big]$, and W_{sb} denotes the searchback window length in number of samples. Note that searchback and threshold selection can also be implemented in other ways, such as thresholding based solely on the noise level [13].

A. Weighted Multiscale Product (WMP) of MZ-DWT

Derivative of Gaussian (dG) approaches are commonly used in the literature for detecting the edges by analyzing the signal at multiple scales. In order to preserve the correlation (and regularities) across various scales, non-orthogonal MZ-DWT [10] is employed. The MZ-DWT of $z[n] \in L^2(\mathcal{R})$ at scale s, where $1 \le n \le N_b$, is given by $W_{2^s} z[n] = z[n] * \phi_{2^s}[n] = \sum_m \phi_{2^s}[m] z[n-m]$, which is equivalent to

$$W_{2^s} z[n] = \left(z * \left(2^s \frac{d\psi_{2^s}}{dn} \right) \right)[n] = 2^s \frac{d}{dn} \big(z * \psi_{2^s} \big)[n] \ , \tag{4}$$

where $\psi[n]$ and $\phi[n]$ are discrete-time approximations to the Gaussian function and its derivative using cubic and quadratic splines, respectively, $*$ denotes convolution, $1 \le s \le S-1$, and $S = \log_2 N_b$. Equation (4) implies that MZ-DWT is analogous to smoothing the signal with Gaussian splines at multiple scales and then estimating the gradients.

As analyzed by Sadler *et. al.* in [11], multiscale product (MP) of MZ-DWT given by $P^{(DWT)}_{S_{opt}}[n] = \prod_{s=1}^{S_{opt}} W_{2^s} z[n]$ can be used for improving the accuracy of edge detection, where S_{opt} is the optimal scale that enhances the regularities. However, it is not guaranteed to observe sharp edges in the UWB energy vector. Since the energy samples do not have a smooth variation, the edges can be mixed with noise samples when the MP-MZ-DWT is used. Poor edge detection performance of this approach in our simulations (which is not surprising due to the discussed issues) motivated us to introduce a weighting function to suppress the edges caused by noise while promoting the edges in the vicinity of the energy-bearing blocks (see Fig. 3)

$$\tilde{P}^{(DWT)}_{S_{opt},\zeta}[n] = \underbrace{\Big(\psi_{2^\zeta}[n] - \min\big\{\psi_{2^\zeta}[n]\big\} \Big)}_{\text{Weighting Function } = G(\zeta)} \times \prod_{s=1}^{S_{opt}} W_{2^s} z[n] \ , \tag{5}$$

where ζ is an arbitrary scale so that the energy in the multipath components is effectively captured in the smoothed signal. The value of ζ is set to 3 in our simulations. The TOA estimate is then given as $\hat{t}_{DWT} = \Big[\underset{1 \le n \le N_b}{\text{argmax}} \big\{ \tilde{P}^{(DWT)}_{S_{opt},\zeta}[n] \big\}\Big] T_b$ for n even, and $\hat{t}_{DWT} = \Big[\underset{1 \le n \le N_b}{\text{argmin}} \big\{ \tilde{P}^{(DWT)}_{S_{opt},\zeta}[n] \big\}\Big] T_b$ for n odd (with the distinction arising in order to calculate the rising edge).

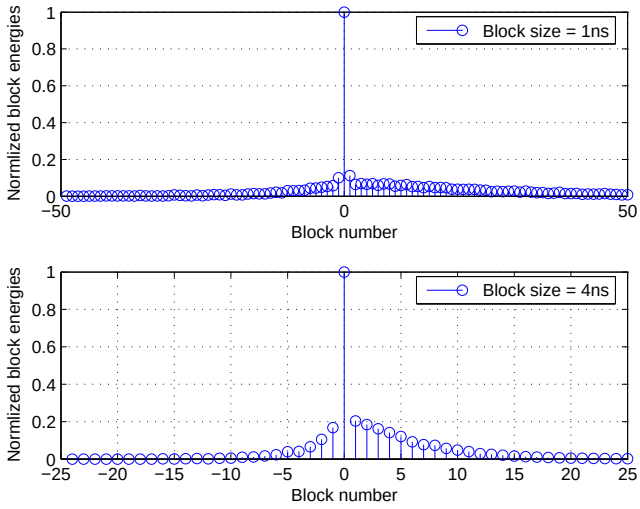

Fig. 4. Mean block energies around the maximum energy block in CM1 for T_b = 1ns and 4ns. Samples with negligible values are discarded on the plots. Time reversed forms of these functions are used for filtering the energy vector prior to block detection (F-MES).

IV. Improving the Accuracy of MES

In this section two filtering techniques that enhance the detection and acquisition (and thus the TOA estimation) performance of the signal by exploiting the energy in the multipath components are presented. The first uses the average energy distribution around the maximum energy block, while the second a bank of scaling filters designed in a dyadic tree structure, which *pushes* the maxima closer to the leading edge of the signal. Upon accurate peak selection, these techniques can be followed by a searchback step for precise TOA estimation.

A. Filtered Maximum Energy Selection (F-MES)

By knowing the average energy distribution around the maximum energy block, one can filter the energy vector to enhance the peaks (and suppress noise components) by collecting the energies present in the neighboring blocks. In Fig. 4 the mean energy distribution around the maximum

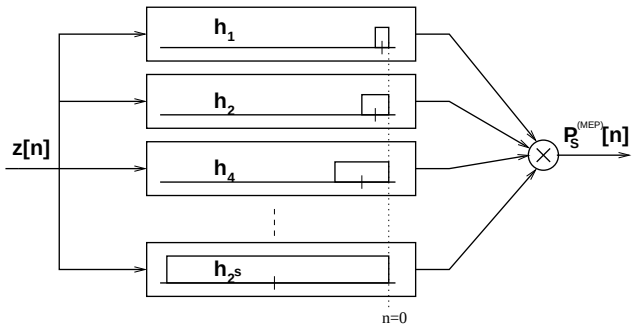

Fig. 5. Filter bank for analyzing the signal energy at different times scales.

energy block is shown for $T_b = 1$ns and $T_b = 4$ns, after averaging over 1000 channel realizations for CM1. The mean block energy values are not significantly different for CM2. In order to capture the energy effectively and characterize the peaks better, one can filter the received energy vector with a time-reversed form of the discrete data in Fig. 4.

B. Multiscale Energy Products (MEP)

Signal energies from coarse to finer time scales can be exploited to improve leading edge detection performance. Using the cross-scale products have two advantages: 1) since the energy samples at different scales are correlated (and the noise samples are uncorrelated), their product is expected to enhance the peaks due to signal existence (and suppress the noise), and 2) by appropriately designing the multiscale filters (see Fig. 5), it is possible to *push* the peak sample closer to the leading edge.

Let $h_{2^s}[n]$ denote the rectangular filter at scale s, given by $h_{2^s}[n] = u[n + 2^s] - u[n]$, where $s = 1, 2, ..., S$ is the scale number ranging from finer scales to coarser, $S = \lfloor \log_2 N_b \rfloor$, and $u[n]$ is the step function. The convolution of $h_{2^s}[n]$ with the energy vector $\underline{z}$ produces energy concentration of our signal at various scales, given by $y_s[n] = \sum_k z[k] h_{2^s}[n-k]$. Since $y_s[n]$ are correlated across different scales, we can use their direct multiplication to enhance the peaks closer to the leading edge of the signal, and suppress noise components, i.e. $P_S^{(MEP)}[n] = \prod_{s=1}^{S} y_s[n]$, where $P_S^{(MEP)}[n]$ denotes the product of convolution outputs from scale 1 (which is the energy vector itself) through scale S. Then, the location of the strongest path is estimated as $\hat{t}_{MEP} = \left\lfloor \underset{1 \le n \le N_b}{\text{argmax}} \{ P_S[n] \} \right\rfloor T_b$.

The timing estimation performance of MEP can be characterized by the statistics of the delay offset between the strongest energy block and first energy block. Let Δ be the distance in terms of the number of blocks between first-arriving energy block and maximum energy block. Using the MEP, the peaks away from the leading edge are effectively suppressed, decreasing Δ. In Fig. 6, cumulative distribution functions (CDF) of Δ before and after the bank of multiscale filters are shown for $T_b = 4$ns at various E_b/N_0. It is observed that especially when the noise variance is high, the MEP lowers Δ, and consequently the error in the TOA estimate. Note that at low E_b/N_0, erroneous selection of the maximum energy block prior to the leading edge becomes more probable, while at high E_b/N_0, the maximum energy samples are usually after the leading edge block.

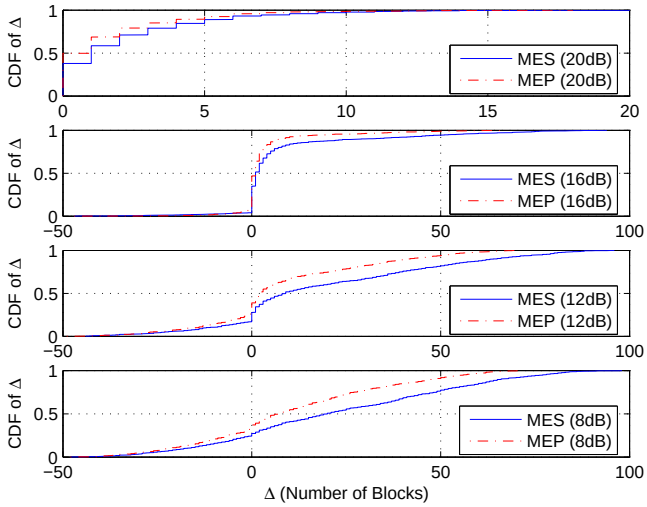

Fig. 6. CDFs of delays between the first energy block and maximum energy block, before and after the bank of multi-scale filters.

V. Results and Discussion

In all the simulations that are presented in this section, the CM1 (residential LOS) channel model of IEEE802.15.4a is employed. The channel realizations are sampled at 8GHz, 1000 different realizations are generated, and each realization has a TOA uniformly distributed within $(0, T_f)$. A raised cosine pulse of $T_c = 1$ns is considered for all scenarios. After introducing uniformly distributed delays, energies are collected within non-overlapping windows to obtain decision statistics. The other simulation parameters are $T_f = 200$ns, $B = 4$GHz, $N_T = 1$, $N_s = 1$, and $W_{sb} = \lceil 15\text{ns}/T_b \rceil$.

The performances of different energy detection based TOA estimation algorithms are analyzed in Fig. 8 for $T_b = 1$ns and in Fig. 7 for $T_b = 4$ns. The ξ_{norm} is set to 0.5 with the assumption that there is no SNR estimate available for appropriate threshold selection (see [12] for detailed analysis for the selection of ξ_{norm} and W_{sb}). It is observed that the TC performs well at high E_b/N_0, and hits a lower error floor compared to MES, while MES is better at higher noise variance. The WMP-MZ-DWT performs better than the MES at high E_b/N_0, however, not as well as the MES-SB. The performance improvement that comes with F-MES is better at higher noise variance. On the other hand, MEP and especially MEP-SB performs well at all E_b/N_0, and does not require estimation of the filter function as in the F-MES case. Using smaller block sizes is seen to yield only slight gains.

In Fig. 9a, MAE performances of MES are analyzed for various T_f values (i.e., ambiguity levels) while $T_b = 1$ns. Even though there is not much variation in the performance at large E_b/N_0, higher N_b may degrade the performance at lower E_b/N_0. In Fig. 9b, performance of MEP-SB was studied when $N_s = 1$ and $N_s = 5$, with identical symbol energies in both cases. It is observed that using multiple pulses per symbol

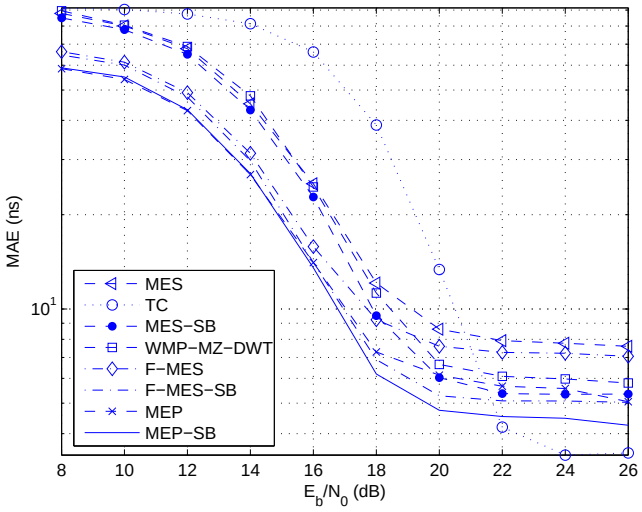

Fig. 7. Absolute error plots for different algorithms with respect to E_b/N_0 (CM1, $T_b = 4$ns).

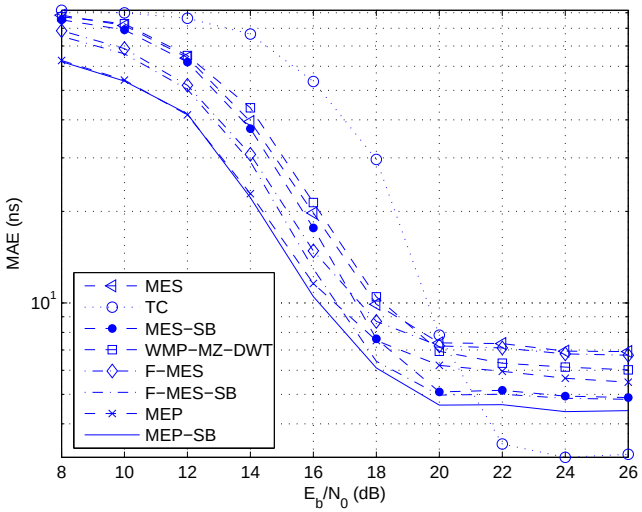

Fig. 8. Absolute error plots for different algorithms with respect to E_b/N_0 (CM1, $T_b = 1$ns).

in essence degrades the performance with an ED approach due to non-coherent combining loss. It can also be seen that multiple symbols can be used to obtain a gain at low E_b/N_0; however, at high SNR in all the cases, similar error floors are experienced.

VI. Conclusion

In this paper, various TOA estimation algorithms for low sampling rate UWB systems based on energy detection are analyzed. A multiscale energy product algorithm which analyzes the energy at multiple time resolutions with hierarchically designed filters is introduced, so that the peaks closer to the leading edge are enhanced. Simulations show that the introduced multi-scale energy product implemented with a search-back outperforms the other algorithms except the TC algorithm at very high SNR.

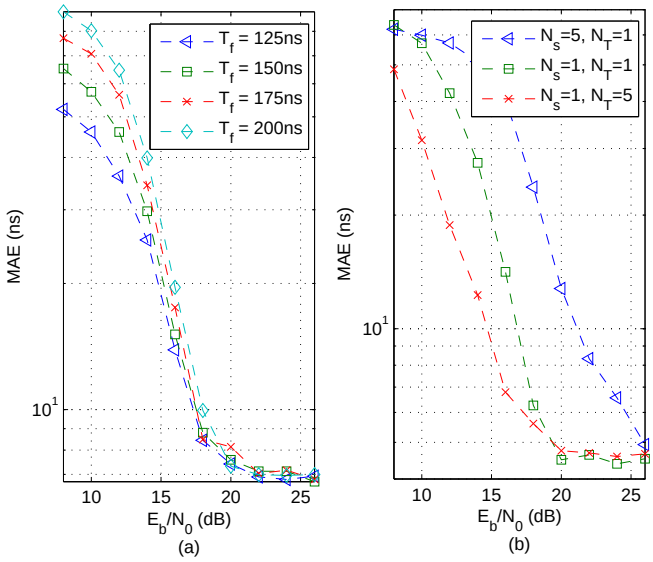

Fig. 9. a) Effect of number of blocks (i.e., initial timing ambiguity) on the performance of MES (CM1, $T_b = 1$ns), b) Comparison of the MAE performance of MES for different N_s and N_T values (CM1, $T_b = 4$ns).

References

[1] R. Qiu, "A study of the ultra-wideband wireless propagation channel and optimum UWB receiver design," *IEEE J. Select. Areas Commun.*, vol. 20, no. 9, pp. 1628–1637, Dec. 2002.

[2] W. Chung and D. Ha, "An accurate ultra wideband (UWB) ranging for precision asset location," in *Proc. IEEE Conf. Ultrawideband Syst. Technol. (UWBST)*, Reston, VA, Nov. 2003, pp. 389–393.

[3] B. Denis, J. Keignart, and N. Daniele, "Impact of NLOS propagation upon ranging precision in UWB systems," in *Proc. IEEE Conf. Ultrawideband Syst. Technol. (UWBST)*, Reston, VA, Nov. 2003, pp. 379–383.

[4] K. Yu and I. Oppermann, "Performance of UWB position estimation based on time-of-arrival measurements," in *Proc. IEEE Conf. Ultrawideband Syst. Technol. (UWBST)*, Kyoto, Japan, May 2004, pp. 400–404.

[5] R. Fleming, C. Kushner, G. Roberts, and U. Nandiwada, "Rapid acquisition for ultra-wideband localizers," in *Proc. IEEE Conf. Ultrawideband Syst. Technol. (UWBST)*, Baltimore, MD, May 2002, pp. 245–249.

[6] J.-Y. Lee and R. A. Scholtz, "Ranging in a dense multipath environment using an UWB radio link," *IEEE J. Select. Areas Commun.*, vol. 20, no. 9, pp. 1677–1683, Dec. 2002.

[7] C. Mazzucco, U. Spagnolini, and G. Mulas, "A ranging technique for UWB indoor channel based on power delay profile analysis," in *Proc. IEEE Vehic. Technol. Conf. (VTC)*, Los Angeles, CA, Sep. 2004, pp. 2595–2599.

[8] S. Gezici, Z. Sahinoglu, H. Kobayashi, and H. V. Poor, *Ultra Wideband Geolocation*. John Wiley & Sons, Inc., 2005, in Ultrawideband Wireless Communications.

[9] A. Rabbachin and I. Oppermann, "Synchronization analysis for UWB systems with a low-complexity energy collection receiver," in *Proc. IEEE Conf. Ultrawideband Syst. Technol. (UWBST)*, Kyoto, Japan, May 2004, pp. 288–292.

[10] A. Mallat and S. Zhong, "Characterization of signals from multiscale edges," *IEEE Trans. Pattern Analysis and Machine Intelligence*, vol. 14, no. 2, pp. 710–732, July 1992.

[11] B. M. Sadler, T. Pham, and L. C. Sadler, "Optimal and wavelet based shockwave detection and estimation," *J. Acoust. Soc. Amer.*, vol. 104, no. 2, pp. 955–963, Aug. 1998.

[12] I. Guvenc and Z. Sahinoglu, "Threshold-based TOA estimation for impulse radio UWB systems," to appear in Proc. IEEE Int. Conf. UWB (ICU), Zurich, Switzerland, Sept. 2005.

[13] I. Guvenc, Z. Sahinoglu, A. F. Molisch, and P. Orlik, "Non-coherent TOA estimation in IR-UWB systems with different signal waveforms," to appear in Proc. IEEE Int. Workshop on Ultrawideband Networks (UWBNETS), Boston, MA, July 2005, (invited paper).